nature COMMUNICATIONS

ARTICLE

Subterranean atmospheres may act as daily methane sinks

Angel Fernandez-Cortes[1,2,3], Soledad Cuezva[1,3], Miriam Alvarez-Gallego[1], Elena Garcia-Anton[1], Concepcion Pla[4], David Benavente[4], Valme Jurado[5], Cesareo Saiz-Jimenez[5] & Sergio Sanchez-Moral[1]

In recent years, methane (CH_4) has received increasing scientific attention because it is the most abundant non-CO_2 atmospheric greenhouse gas (GHG) and controls numerous chemical reactions in the troposphere and stratosphere. However, there is much that is unknown about CH_4 sources and sinks and their evolution over time. Here we show that near-surface cavities in the uppermost vadose zone are now actively removing atmospheric CH_4. Through seasonal geochemical tracing of air in the atmosphere, soil and underground at diverse geographic and climatic locations in Spain, our results show that complete consumption of CH_4 is favoured in the subsurface atmosphere under near vapour-saturation conditions and without significant intervention of methanotrophic bacteria. Overall, our results indicate that subterranean atmospheres may be acting as sinks for atmospheric CH_4 on a daily scale. However, this terrestrial sink has not yet been considered in CH_4 budget balances.

[1] Department of Geology, National Museum of Natural Sciences (MNCN-CSIC), 28006 Madrid, Spain. [2] Department of Earth Sciences, Royal Holloway, University of London, Egham, Surrey TW20 0EX, UK. [3] Geomnia Natural Resources SLNE, 28003 Madrid, Spain. [4] Department of Environment and Earth Sciences, University of Alicante, San Vicente del Raspeig, 03690 Alicante, Spain. [5] Department of Agrochemistry, Environmental Microbiology and Soil Conservation, Institute of Natural Resources and Agricultural Biology (IRNAS-CSIC), 41012 Seville, Spain. Correspondence and requests for materials should be addressed to A.F-C. (email: acortes@mncn.csic.es).

Methane (CH_4) is currently the most abundant non-CO_2 greenhouse gas (GHG) in the atmosphere, reaching a global average concentration of $\sim$1,800 p.p.b. at mid-northern latitudes[1]. Despite significant research progress in recent years, large uncertainties remain about the CH_4 budget and its evolution over time because there is a lack of knowledge about CH_4 sinks and sources[2–5]. Superimposed on the long-term trend of increasing atmospheric CH_4, there is significant interannual variability[1,6,7], and the sources of variation remain controversial[8].

Current CH_4 estimates account for $\sim$22% of the total forcing potential of all long-lived GHGs[9]. By weight, CH_4 is 28 times more effective at trapping heat in the atmosphere than CO_2 over a 100-year period[10]. Sensible mitigation strategies also require a quantitative understanding of the CH_4 budget regarding emissions and sinks[11]. The total global emissions of CH_4 are constrained reasonably well by atmospheric observations and estimates of its lifetime, based on multiple atmospheric CH_4 inversion models (top–down studies). However, the uncertainties concerning emissions/consumption from individual sources/sinks[12] are greater, and they are poorly constrained by the current atmospheric observation network[6]. Some unaccounted sinks (or sources) could contribute the global CH_4 budget and its long-term variations.

The Earth's surface exerts its influence on the free atmosphere through the atmospheric boundary layer. This lowest portion of the atmosphere ranges from a few tens of metres to 1–2-km deep[13]. The subsurface atmosphere is usually overlooked as an important part of this boundary layer. At the top of the subsurface layer in the vadose zone (below the subsoil and above the groundwater table) highly specific biogeochemical processes occur, which may act as regulators of gas exchanges between the surface and the free atmosphere.

The uppermost part of the vadose zone may contain large amounts of underground air, that is, a CO_2-rich air reservoir permeating the unsaturated zone[14]. Underground air occupies air-filled caves, empty-water pores, cracks and voids in bedrock or unconsolidated sediment, some of which exhibit a direct connection to the open atmosphere[15]. The gas exchange between the bulk of the atmosphere and small air-filled locations, for example, fissures, cracks and voids, is minor compared with the exchange that occurs between large shallow caves and the open atmosphere. Hence, shallow caves can be thought of as small-scale representations of the uppermost part of the vadose zone, where there is intense gas exchange with the atmosphere. Shallow caves may largely represent the volume of underground air that is distributed widely across continental ecosystems.

Furthermore, shallow caves are favourable for *in situ* monitoring of gaseous exchange processes at the subsurface. They are easily accessible natural macropores that can store edaphic or atmospheric gases several tens of metres below the soil. These shallow vadose environments below the soil show significant seasonal and even daily variations in the gas composition of underground air[16–18], which involves the exchange of large amounts of other GHGs in addition to $CO_2(g)$ with the lower troposphere[15,19]. However, there is great uncertainty regarding the behaviour and lifetime of CH_4 in these shallow vadose environments.

Here to better understand the behaviour and lifetime of the CH_4 in subsurface environments located in the vadose zone, spatiotemporal spot measurements and continuous geochemical tracing of air (in the atmosphere, soil and cave air) have been carried out by monitoring CH_4, CO_2 and stable carbon isotopic $\delta^{13}C[CO_2]$ using cavity ring-down spectroscopy (CRDS). In total, >1,000 air samples have been analysed for seven caves located in Spain. The caves exhibit a wide range of geographic, geologic and climatic features (Supplementary Table 1). For each cave, the sampling was conducted in underground air, soil air and external atmosphere. Comprehensive microclimatic monitoring of the exterior, soil and cave atmosphere was conducted simultaneously with GHG tracking. In addition, potential methanotrophy at each subsurface site was assessed by tracking the presence of methane-oxidizing bacteria (MOB) using specific DNA primers for methanotroph *pmoA* sequences[20]. The overall results show that complete consumption of CH_4 is favoured in the subsurface atmosphere under near vapour-saturation conditions without significant intervention of methanotrophic bacteria. The oxidative capacity of underground air must be related to its high density of ions, some of which are likely to react with CH_4. Overall, our results indicate that subterranean atmospheres may be acting as sinks for atmospheric CH_4 on seasonal and daily scales.

Results

GHGs in underground air. Spot air samplings were conducted during short surveys at all fieldwork sites, within a predefined network of points that were spatially distributed from the entrance to the innermost accessible areas of the cavities. Exterior and soil air were also sampled at fixed locations throughout the day, and, preferably, during maximum (midday) and minimum photosynthetic activity (early morning). Further details about the air-sampling procedures are found in Methods section. Air samples were analysed in the laboratory within 48 h of sampling for determine CO_2 and CH_4 concentrations and the isotopic $\delta^{13}CO_2$ signal using CRDS technology.

The comparison of CO_2 and CH_4 enables assessment of the influence of the exterior atmosphere and soil on the gas contents of cave air, that is, the degree of isolation of the subsurface environment. Figure 1 shows the variations in the concentration of CH_4 and CO_2 in underground air relative to their local atmospheric levels for the main four caves studied. Supplementary Figure 1 shows the extended results for the entire set of caves studied, covering a wide latitudinal transect of the Iberian Peninsula that includes different environmental features, which are summarized in Supplementary Table 1. There is an inverse relationship between the two GHGs along a subsurface–soil–atmosphere profile. Both soil and cave air exhibit a lower concentration of CH_4 compared with local atmospheric background and regional CH_4 levels (1.83–2.05 p.p.m. for the period 2011–2012, based on records for Central Spain from NOAA). An opposite pattern is found for CO_2 in cave air, which is consistent with the usual magnitude of the $CO_2(g)$ reservoirs found in shallow caves[21,22], presenting average values that are 10–100 times the current mean atmospheric concentration (0.04% vol). The overall results indicate a higher CH_4 depletion rate (from -0.1 to -0.4 p.p.m. for each 100 p.p.m. increase in CO_2) under low-moderate contents of CO_2 (<1,000 p.p.m.). Furthermore, this CH_4 depletion rate rises in highly ventilated caves (for example, the Ojo Guareña and Sidron caves) within a narrow increment of CO_2 (500→700 p.p.m.). Shallow caves where there is intermediate and seasonal ventilation of underground air (for example, the Altamira Cave) display a lower rate of decreases in CH_4 contents (lower than -0.1 p.p.m. of CH_4 for each 100 p.p.m. increment of CO_2), especially in cave locations subjected to a stronger influence of the external atmosphere, but showing considerable CO_2 levels (1,000–3,000 p.p.m.). Most isolated caves with the lowest ventilation rates (for example, the Castañar Cave) present a steady state, with practically null CH_4 levels, thus suggesting that complete removal of CH_4 from the underground air occurs once a CO_2 concentration above 3,000 p.p.m. is reached, which is observable in the deepest
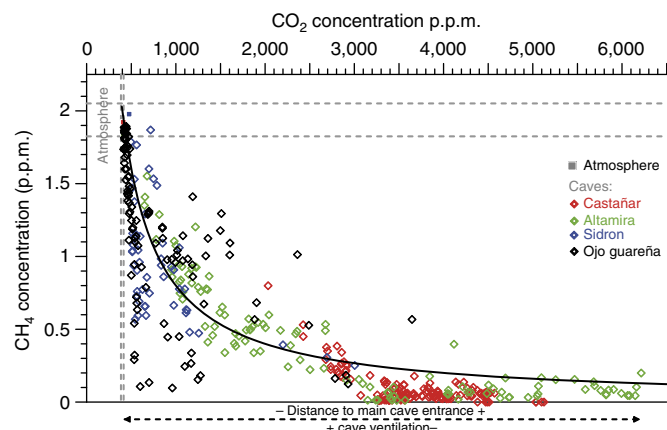
Figure 1 | Variations in the concentrations of GHGs in underground air.
Caves (open diamonds), local atmosphere (solid squares). The grey dashed lines indicate the regional levels of the atmospheric CH_4 and CO_2 Dry Air Mole Fractions from the NOAA earth system research laboratory (ESRL) global monitoring division (GMD) Carbon Cycle Cooperative Global Air Sampling Network as a reference[62,63]. In particular, the grey dashed lines correspond to representative minimum and maximum data from the well-mixed troposphere from central Spain (Centro de Investigación de la Baja Atmósfera, University of Valladolid, 41.81° N, 4.93° W, 845 m a.s.l. (above sea level)) for the period 2011–2012 coeval to the cave air samplings.

remote cave locations. The dynamically ventilated caves show greater spatiotemporal variability in their CO_2 and CH_4 concentrations, which is shown by the fact that the paired data for both the parameters are more scattered compared with caves in which there is limited ventilation of underground air.

The CH_4 depletion rate and its variation relative to CO_2 content in underground air (Fig. 1) were, therefore, key parameters for assessing the ventilation of subterranean atmospheres. In highly ventilated caves, a significant volume of air circulates daily, and, consequently, there is a nearly continual contribution of air to the subterranean atmosphere, which has lower CO_2 content and atmospheric levels of CH_4. Hence, the CH_4 depletion rises with slight changes in CO_2 close to atmospheric background. Conversely, in the most isolated caves, CO_2 reaches high concentrations because air exchange with the outer atmosphere is negligible. Thus, the removed CH_4 is not rapidly replenished. As a result, the CH_4 depletion rate tends to become negligible as the CO_2 content of cave air rises.

The CO_2 concentration in cave air is determined by the mixing of background atmospheric CO_2 with soil-produced CO_2, and the mixing process fits a Keeling model with a mean y-intercept value ranging from −25 to −28‰ for the caves studied (Fig. 2). The CO_2-soil recharge by diffusion is more of an important factor at the most isolated subterranean sites, such as Castañar and Altamira caves, where the cave air usually has a higher CO_2 concentration and $\delta^{13}C[CO_2]$ below −20‰ with respect to other caves. Conversely, the lower CO_2 concentration and the $\delta^{13}C[CO_2]$ value that tends toward the local atmospheric background (∼9%), as measured in Sidron and Ojo Guareña caves, indicates rapid air renewal that allows the air to become well-mixed with the atmosphere.

Seasonal variation of CH_4 in dynamically ventilated caves.
Multi-parameter monitoring was conducted for the cave–soil–atmosphere (main climatic data and gas composition) and geochemical tracing was performed using $\delta^{13}C–CO_2$ to assess the climate-driven fluctuations of GHGs in the subsurface and to determine the spatiotemporal patterns of exchange between soil

and atmosphere. A 3-km-long area of the subterranean system of Ojo Guareña (northern Spain) was chosen for field research. The Ojo Guareña cave system is one of the longest caves in Europe and is the most dynamically ventilated cave site of all the sites studied, according to our most recent studies[23].

Cave air ventilation increased from the end of the summer to early winter in the case of the Ojo Guareña subterranean system (Fig. 3; Supplementary Fig. 2). During winter, the outside air temperature is lower than the inside air temperature, and, consequently, the outside air density is higher than the cave air density. This favours advective air movement, primarily through the cave entrance and other host-rock discontinuities. Therefore, a higher proportion of CH_4-enriched air was progressively transferred from the open atmosphere to the cave during the winter months than in summer. Higher CH_4 depletion with narrow increases of CO_2 indicates a prevailing influx of outer air into the cave, and the CH_4 consumption rate consequently increases from summer to winter. The CH_4 depletion rate in underground air with an increasing CO_2 concentration is significantly higher than the rate of CH_4 consumption through soil MOB. The CH_4 depletion, coeval to increments of CO_2 concentration in underground air, is higher in cave locations that are closer to the surface (CH_4 concentration above 0.75 p.p.m.) and decreases in deeper and more isolated locations (CH_4 concentration below 0.5 p.p.m.). In the most isolated locations, CO_2 diffusion from the soil prevails over the influx of exterior air with the atmospheric CH_4 levels and lower CO_2 concentrations.

**Daily variation of CH_4 consumption in ventilated caves.** *In situ* and real-time measurements of CO_2, CH_4 and $\delta^{13}CO_2$ were carried out during an intensive field campaign in Altamira Cave. This intensive monitoring period was examined to assess the complete daily cycles of the GHG mixing ratios through comprehensive real-time logging using the same field-deployable CRDS analyser. The results summarized in Fig. 4 correspond to data records from the field campaign conducted in September 2011 (end of summer). In Methods section are summarized the technical procedures applied in the real-time air monitoring deployed in the field sites, including the number and frequency of records and the $\delta^{13}C–CO_2$ calculation.

The interaction of three air masses (soil–cave–exterior) is driven by soil-derived CO_2 diffusion into the cave and by the advective mixing of the cave with exterior air[18]. The diffusive process increases cave CO_2 concentration and decreases $\delta^{13}C[CO_2]$, to the extent that biological respiration in the soil causes an accumulation of CO_2 molecules with a lighter carbon isotopic signature. In contrast, advective mixing causes the CO_2 levels to decrease and causes the isotopic signal to increase because it causes the uptake of air with an atmospheric CO_2 level and a heavier $\delta^{13}C[CO_2]$ compared with both soil and cave air. The diffusive flux usually increases with soil CO_2 production, and the advective flux is driven by outer–inner density gradients. Both of these drivers are primarily regulated by the external meteorological conditions.

The monitoring results confirmed that the driving forces for the increases in CH_4 in underground air are the same as for the declines in CO_2 levels, and the daytime increase of the CH_4 content of underground air ($+0.04$ p.p.m. h^{-1} on average with the maximum reaching $+0.11$ p.p.m. h^{-1}) is, therefore, synchronous with decline in the CO_2 levels and an increase in $\delta^{13}C[CO2]$ (Fig. 4), which points to an air inlet from the outside atmosphere. Consequently, the maximum values of CH_4 begin to be reached after sunset but usually remain below the background atmospheric levels. On the contrary, during the night, the CH_4 depletion of underground air is coeval with an increase in CO_2
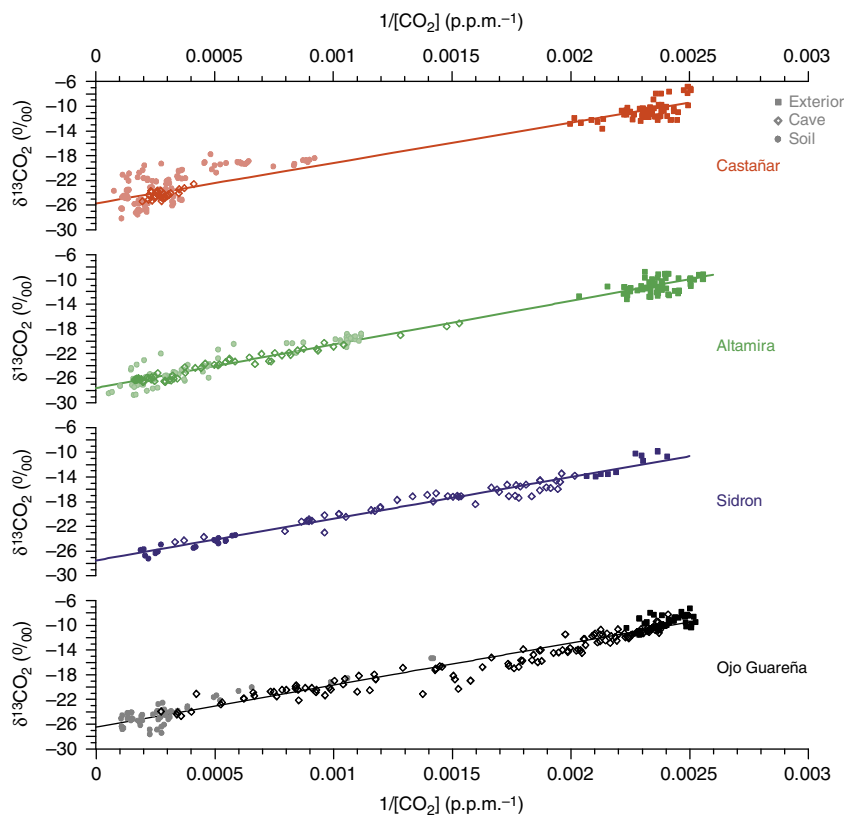
Figure 2 | Keeling models for the subterranean atmosphere at each cave site. Isotope ratios are plotted against the inverse of CO_2 concentration for all air samples (see Supplementary Table 1, and notice the number of air samples for each fieldwork site), distinguishing a three-component mixture: background atmosphere (solid squares), cave air (open diamonds) and soil air (solid circles). The y-intercept of the Keeling models corresponds to the carbon isotope composition for the integrated value of the CO_2 sources in the ecosystem: $-25.71‰$ for Castañar cave ($R^2 = 0.93$), $-27.59‰$ for Altamira cave ($R^2 = 0.98$), $-27.50‰$ for Sidron cave ($R^2 = 0.97$) and $-26.48‰$ for Ojo Guareña cave ($R^2 = 0.96$). As the distance of the cave air samples from the y-intercept of the Keeling models increases, there is greater ventilation and greater influence of the external atmosphere. Conversely, when CO_2 concentration is high and $\delta^{13}C[CO_2]$ tends toward the y-intercept, the gas enters by diffusion and has a mainly edaphic origin.
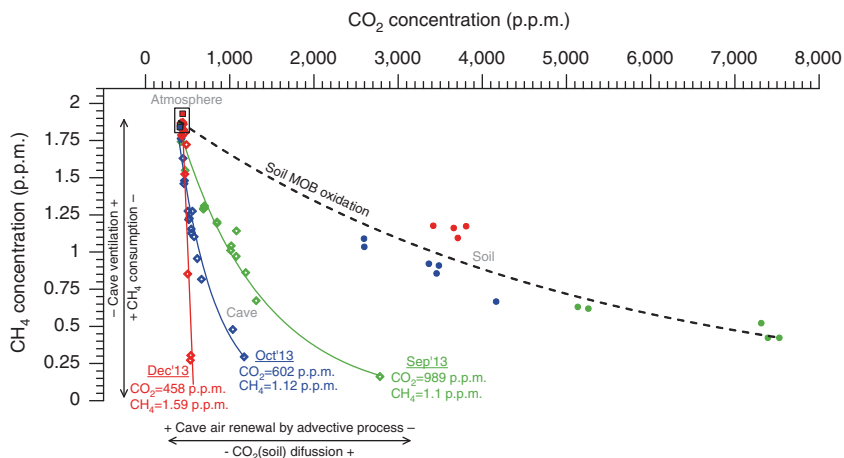
Figure 3 | Seasonal variability of GHGs in a dynamically ventilated cave. Cave (Ojo Guareña, Spain) air samples (open diamonds), soil air samples (solid circles) and atmospheric air samples (solid squares). Each colour corresponds to an air sampling date in 2013: September (green), October (blue) and December (red). The dashed black line represents CH_4 oxidation by soil MOBs as a function of CO_2 concentration in the soil air ($[CH_4, p.p.m.] = 2.04 \times exp(-2.09 \times 10^{-4} \times [CO_2, p.p.m.])$, $R^2 = 0.96$). Coloured lines correspond to the functions for each monthly set of paired CH_4 and CO_2 data for the air from cave environments; 18 September 2013: $[CH_4, p.p.m.] = 2.72 \times exp(-9.95 \times 10^{-4} \times [CO_2, p.p.m.])$, $R^2 = 0.98$, 29 October 2013: $[CH_4, p.p.m.] = 4.35 \times exp(-2.3 \times 10^{-3} \times [CO_2, p.p.m.])$, $R^2 = 0.96$) and 10 December 2013: $[CH_4, p.p.m.] = -1.35 \times 10^{-2} \times [CO_2, p.p.m.] + 7.79$, $R^2 = 0.82$. The slope of these coloured lines is indicative of the consumption of atmospheric CH_4 due to the influx of outer air into the cave via advective processes. In the case of the exponential functions, an increase of the coefficient multiplying the CO_2 concentration implies a higher CH_4 depletion. The average concentrations of CH_4 and CO_2 in underground air for each month is indicated, considering the entire set of 15 cave-air-sampling points for each field campaign.
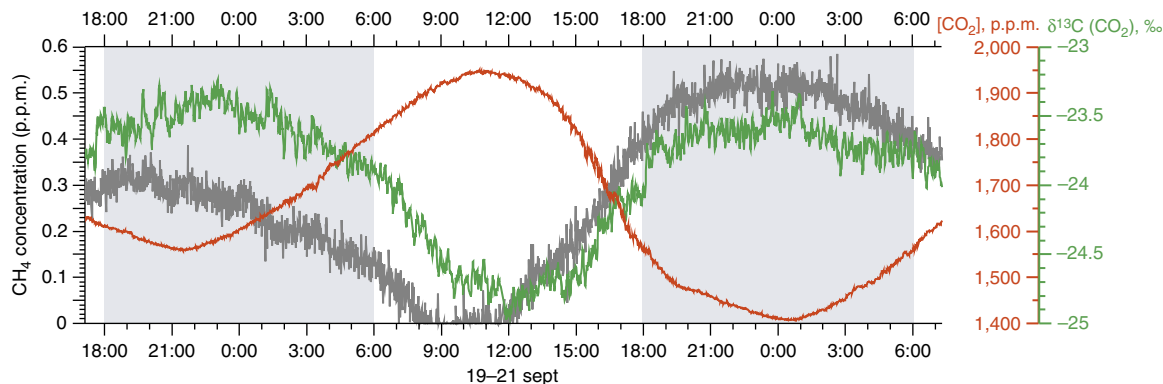
Figure 4 | Daily variations of CH_4 and CO_2 contents and the carbon isotopic signal in underground air. Data from the Altamira Cave (from day 19 to 21 September 2011). The shaded area represents the night-time period delimited by null solar radiation, in accordance with ancillary monitoring parameters (the applied methods and full time series are described by Garcia-Anton et al.[18]). All records are reported relative to Greenwich Mean Time.

contents and a decrease in $\delta^{13}C[CO2]$, which indicates the existence of a CO_2 gas inlet with an edaphic origin, primarily via diffusion. Conversely, the gradient of CH_4 contents between the soil and cave is not sufficient to enable an influx to underground air, due to the likely CH_4 consumption in soil through MOBs action. In the absence of nocturnal influx of atmospheric CH_4 via advective forces, CH_4 consumption mechanisms in the underground air seem to be triggered, the CH_4 content consequently decreases to an average rate of $-0.03\,p.p.m.\,h^{-1}$ (maximum of $-0.05\,p.p.m.\,h^{-1}$), reaching $0\,p.p.m.$ early in the morning (8:30 h Greenwich Mean Time).

Tracking the presence of MOB. We evaluated whether the CH_4 oxidation pattern by soil MOB was repeated in cave sediments. Microbiological sampling was conducted to assess the presence or absence of MOBs in the edaphic profile at the exterior and in sediments and on rock surfaces in the cave at each monitored field site. The collected samples were analysed through an ordered set of techniques, including nucleic acid extraction and PCR amplification, cloning and sequencing and sequence analyses (see Methods section for details of these analytical techniques).

The results obtained through microbiological sampling of cave sediments from the main four caves studied revealed the presence of *Methylocapsa aurea* (FN433470), *Methylomicrobium album* (EU722431), *Methylococcus capsulatus* (AE017282) and methanotrophs of the K1-1 (AF547174) and K3-16 (AF547178) strains only in the samples from the Altamira, Sidron and Ojo Guareña caves, mainly in locations where CH_4 usually reaches concentrations near to the atmospheric background levels. These analyses did not detect methanotrophs in remote subterranean locations or poorly ventilated caves, such as the Castañar Cave, where CH_4 is absent or present in minimal concentrations (below the accuracy threshold) throughout the year.

CH_4 removal in relation to other environmental parameters. Our initial measurements of the density of ions in Castañar Cave (roughly 200×10^3 ions per cm^3) revealed an extraordinary degree of air ionisation, ~100–1,000 times greater than in the local open atmosphere. The high density of ions in this cave atmosphere persists throughout the year, in the absence of CH_4. This leads us to hypothesize that the oxidative capacity of underground air is related to its high density of ions, some of which likely are able to react with CH_4.

In light of these preliminary observations, a specific and detailed multiparametric field study was conducted in the cave that had the highest ventilation rate, Ojo Guareña Cave[23]. This

underground system was chosen because positive concentrations of CH_4 were always recorded throughout the year, in contrast to other isolated underground sites such as Castañar Cave. In Castañar Cave, CH_4 is hardly detected at all throughout the annual cycle. The field study included the monitoring of gas composition (air ion concentration, CH_4, CO_2 and its carbon isotopic signal) and microclimatic parameters (temperature and relative humidity). Spot air sampling was conducted during a short survey of the cave air, soil air and open atmosphere using the same procedures described above. The density of ions in underground air as measured simultaneously with environmental monitoring and air sampling using a handled air ion counter (AlphaLab Air Ion Counter, UT, USA).

Figure 5 summarizes the spatial variation of air ion concentration and CH_4 content in the underground air of Ojo Guareña Cave. The negative and positive ions have the same concentration range (5–45×10^3 ions per cm^3) and an identical spatial distribution. Hence, Fig. 5 includes only the spatial distribution of negative ions (the positive ions show the same distribution). The spatial distributions of other ancillary parameters are displayed in Supplementary Fig. 3, including air temperature, CO_2 concentration and CO_2 carbon isotopic signal, $\delta^{13}C[CO_2]$ (the relative humidity of cave air remains close to a steady state of saturation, 100%, in the entire network of air-sampling points). Radon concentration in the air was continuously monitored in two cave locations with opposite ventilation patterns[23]. The levels of radon observed during the 24-h cycle immediately before the fieldwork campaign ranged from 693 [454–1,033] $Bq\,m^{-3}$, at the final stretch of the western gallery near the cave entrance, to 966 [760–1,386] $Bq\,m^{-3}$ in the dead-end gallery located in the northeast sector of the subterranean system (Fig. 5a).

The minimum air ion concentrations, for both negative and positive ions, were measured close to the cave entrances, with values slightly higher than those observed in the exterior atmosphere. Medium values (15–25×10^3 ions per cm^3) were measured in the cave sector between the entrances, where bidirectional air circulation is noticeable throughout the year, accordingly to our continuous monitoring studies[23]. The highest ionisation levels of cave air were found in the eastern dead-end gallery of the cave, coinciding with the highest CO_2 ($>2,500\,p.p.m.$) concentration, the lowest levels of $\delta^{13}C[CO_2]$ ($<-23‰$) (Supplementary Fig. 3) and the maximum radon activity in the air, which indicates less influence of the aerodynamic processes that control cave air renewal.

The spatial pattern of CH_4 concentration is the opposite of the air ion concentration pattern (Fig. 5d). In accordance with

the estimated spatial distribution of the CH_4 content in underground air, ∼80% of the cave surface (∼7,160 m²) has a CH_4 concentration below the levels found in soil air (0.89–1.74 p.p.m.), with almost null values in the north-eastern galleries far from the cave entrances. The remaining 20% of the cave surface is located near entrances and has the CH_4 levels close to the local atmospheric background (1.77–1.96 p.p.m.). The atmospheric

CH_4 is reduced to ∼1 p.p.m. when moving from the accesses to the subterranean system to the highly ventilated sector between both cave entrances.

A linear function fits the data describing CH_4 depletion in the underground air as it becomes increasingly ionized (Fig. 5d). A CH_4 removal of 0.26 p.p.m. in the subsurface atmosphere is observed as the air ion concentrations, both positive and negative,
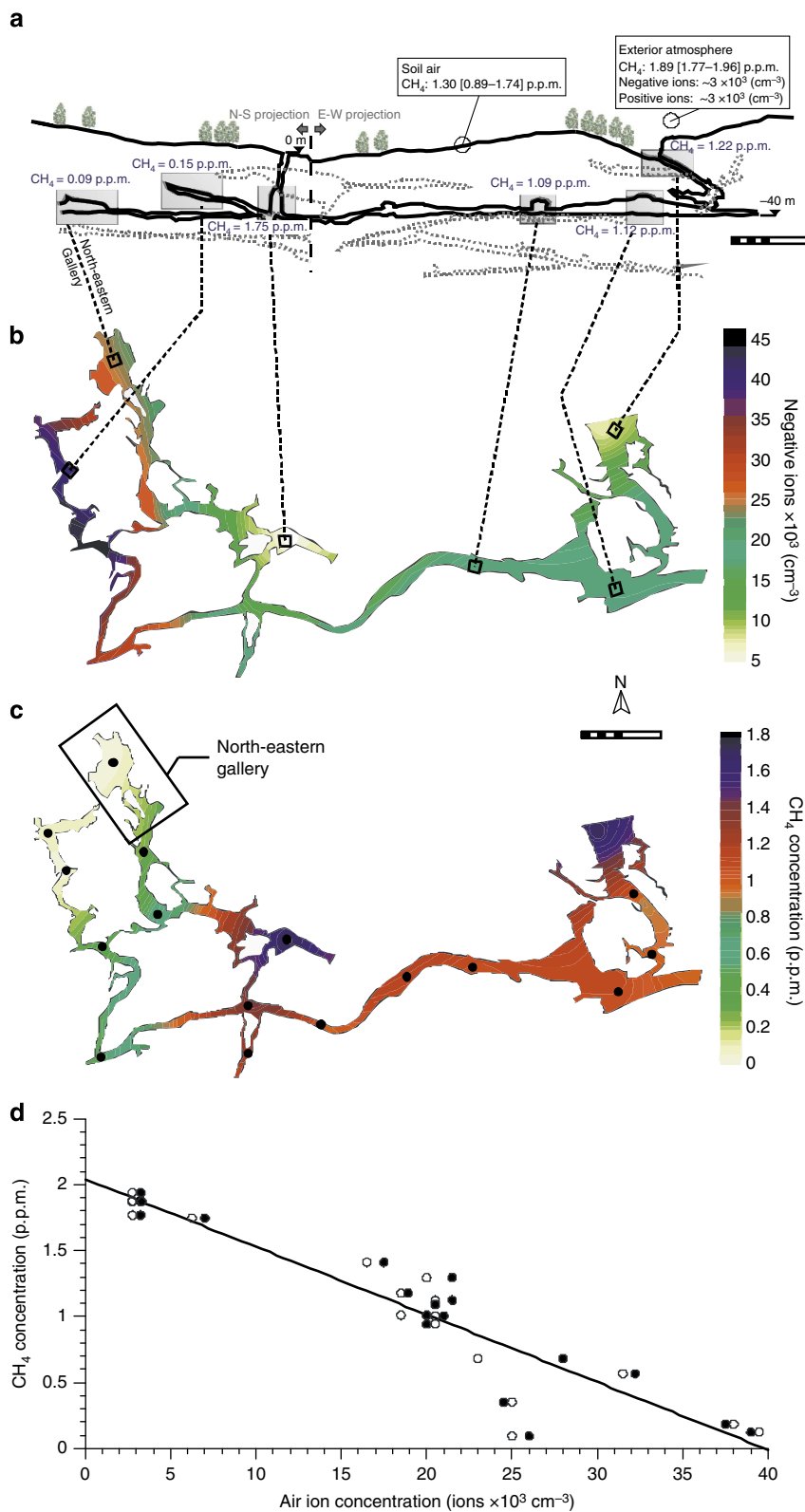
increase to 5×10^3 ions per cm^3. Depletion of local atmospheric CH_4 ranging from 1.17 to 1.36 p.p.m. is expected based on the averaged degree of ionisation of the subsurface atmosphere at the fieldwork site (~ 23.3 ions · per cm^3, for both positive and negative ions).

Some points differ to this linear trend, that is, they show a low CH_4 concentration, below 1 p.p.m., with an intermediate air ion concentration ($\sim 25 \times 10^3$ ions · per cm^3; Fig. 5d). These points correspond to air-sampling points located in a north-eastern gallery connected with the rest of the subterranean system (Fig. 5). This cave sector is under the influence of air exchange processes that cause an influx of underground air that is heavily depleted in CH_4, but less ionized than the bordering galleries with similar minimum CH_4 concentrations. Therefore, this intermediate air ion concentration ($\sim 25 \times 10^3$ ions · per cm^3) seems to be enough to cause CH_4 concentrations below 0.5 p.p.m. The values of the ancillary key parameters (lower air temperature, higher CO_2 content and a reduced $\delta^{13}C[CO_2]$ signal, as shown in Supplementary Fig. 3) confirm the distinctive higher ventilation of this cave sector relative to the surrounding galleries. The northernmost galleries with no air circulation are less influenced by the air renewal processes and that affects their maximum air ion concentration and minimum CH_4 concentration.

Discussion
The CH_4 consumption in underground air is markedly higher than CH_4 depletion in soil air due to methanotrophy. In addition, the CH_4 consumption rate in underground air varies depending on the CH_4 input ratio from the atmosphere, which is determined by the intensity of cave air ventilation represented by the CO_2 levels. Real-time measurements have revealed that consumption of atmospheric CH_4 in subsurface environments is even faster than at the soil surface, within just a few hours. Thus, the CH_4 concentration in underground air varies throughout day, showing a very similar pattern to the carbon isotope $\delta^{13}C[CO_2]$ signal, but presenting an opposite pattern to CO_2 contents. In the case of CO_2, its movement occurs through a combination of advection and diffusion processes, at both daily[17,18] and seasonal[24,25] timescale.

The outer air that enters the cave, mainly during daylight hours, is fully depleted of CH_4 within a few hours, and this underground air reservoir subsequently partially advects upwards and exhales out into the atmosphere on a daily basis. Therefore, the variation in CH_4 abundance reveals itself as a key parameter for assessing the ventilation of subterranean atmospheres, as in the case of other tracer gases (radon). This circadian pattern of both GHGs has been consistently observed over different seasons, and, preferentially, in dynamically ventilated caves during periods of the year with drier conditions. These results are fully consistent

with the subsurface environments acting, at a short-term scale, as cleaning filter for atmospheric CH_4 coming from air that directly enters the subsurface, bypassing the edaphic layer via air mass advection (for example, through a cave entrance), far from the influence of biochemical oxidation by soil CH_4 and methanotrophic bacteria.

The main mechanism responsible for the complete consumption of CH_4 in the studied underground environments must be something other than the previously suggested bacterial oxidation mechanism[26,27] because the remaining null CH_4 concentration is not sufficient to satisfy energy requirements for the maintenance and growth of methanotrophic populations. In our MOB tracking, we did not detect methanotrophs in the cave sediments from poorly ventilated subterranean sites. This is consistent with the fact that we found no significant concentrations of CH_4 throughout the year. This suggests that an agent other than methanotrophs should also consume CH_4 at subsurface locations where the gas is absent for long periods. A negative correlation between CH_4 concentration and the density of ions in the cave air has been observed in highly ventilated caves (for example, Ojo Guareña). In this context, charged airborne particles with electrical mobility (primarily, inorganic ions) could play a significant oxidizing role.

The small ions exist all the time in the atmosphere, and the average concentrations of positive and negative small ions are typically 0.2–2.5×10^3 cm^{-3} (ref. 28). However, concentrations up to 45×10^3 cm^{-3} have been observed in the dynamically ventilated caves studied (for example, the Ojo Guareña Cave). Some anomalous high concentrations of ions have previously been reported in other underground locations[29]. During their lifetime of about 100 s, small ions undergo a series of ion-molecule reactions and continuously change their chemical identity[30]. The negative ions have greater affinity for the condensing vapours[31,32], consequently the ion-mediated particle formation mechanisms are expected to be important in locations with high relative humidity[33,34], close to 100% (for example, in caves). The small air ions are usually composed of the central primary ion and surrounding 4–10 molecules of water, depending on humidity, temperature, actual concentration of trace gasses[35] and polarity of the ions.

The main natural sources of small ions are air molecule ionization by radon decay, gamma and cosmic radiation, all of them exhibiting strong spatial and temporal variations[28]. The enhanced radon activity concentration causes the variation in the ionization rate, increasing the small ion concentrations observed near the ground at certain sites, especially where there is an accumulation of radon in the air[29,36–38]. The ionization rate via radon decay is highly sensitive to the elevation from the ground, so it is larger closer to the ground[39].

Figure 5 | Spatial variation of air ion concentration and CH_4 concentration in underground air. Data from a dynamically ventilated cave (Ojo Guareña, Spain). Sampling campaign of 8 October 2014. Length of scale bars is 50 m. (**a**) Detailed cross-sections of cave galleries in relation to surface geomorphology and the main entrances to the subterranean system (solid black line represents the studied galleries; the ends of these galleries continue with the rest of the subterranean system, which is not drawn; and the dotted lines show the locations of other cave levels). Data on air ion and CH_4 concentrations in the atmosphere and in soil air are displayed in relation to the average CH_4 concentration of the main cave sectors (shaded rectangles). (**b**) Spatial distribution of negative ions (both negative and positive ions have the same range of concentration, 5–45 $\times 10^3$ ions per cm^3, and an identical spatial distribution. Thus, only the spatial distribution of the negative ions is displayed to avoid redundancy). (**c**) Spatial distribution of CH_4, indicating a network of points (filled black circles) at which spot sampling of cave air was conducted. CH_4 data come from the spot air sampling during short surveys and the subsequently GHG analyses on lab using the CRDS technique. The spatial maps for each parameter were constructed using geostatistical gridding based on an ordinary point kriging method, with a linear variogram model and without anisotropy constraints during interpolation (distance between the estimated points ranging from 3 to 5 m). The north-eastern gallery connected with the rest of the subterranean system is shown in both maps. (**d**) Functional relationship between air ion concentration (open circles: negative ions and closed circles: positive ions) and CH_4 concentration in underground air. The continuous black line corresponds to a linear function that best fits the prevailing CH_4 depletion in the underground air, which occurs as the air becomes increasingly ionized ([CH_4, p.p.m.] $= -0.051 \times$ [ions $\times 10^3$, cm^{-3}] $+ 2.04$, with $R^2 = 0.87$). Air ion concentration refers to either positive ions or negative ions.
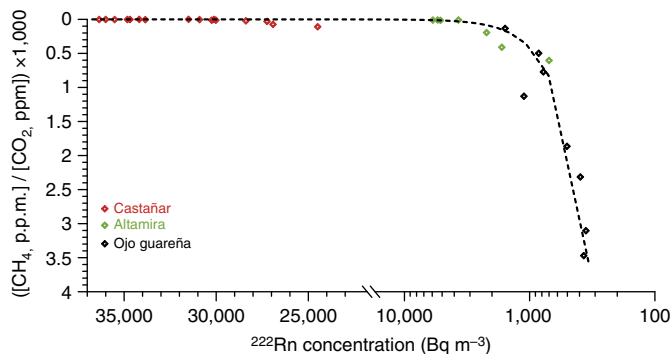
Figure 6 | Variation in the ratio of the concentrations of both greenhouse gases in underground air in relation to radon activity. The ratio of the concentrations of CO_2 and CH_4 is directly proportional to the intensity of ventilation process of the subsurface atmosphere. The coloured points correspond to paired data on the average concentrations of both parameters in the underground air for each field campaign of spot air sampling. Three main caves were considered to display this functional relationship, namely, Castañar, Altamira and Ojo Guareña. Continuous monitoring of radon activity in the underground air was conducted in these caves. The x axis for radon concentration in underground air is divided into two parts (with linear and logarithmic scale, respectively) to show the variations of the ratio of the concentrations of CO_2 and CH_4 in a very broad range of radon activity. The continuous black line corresponds to a second-order hyperbola that best fits the functional relationship between the ratio of the concentrations of both the greenhouse gases (CO_2 and CH_4, in p.p.m.) and its radon activity (^{222}Rn in $Bq\,m^{-3}$), ($[CH_4] \cdot [CO_2]^{-1}) \cdot 1,000 = 4.108 \times 10^5 \cdot ([^{222}Rn] + 0.045)^{-1}$, with $R^2 = 0.96$).

Recent indoor experiments showed that determining positive air ion concentration could be an alternative method for evaluating radon activity concentrations[40]. It has been also observed that the source rate of small ions by radon activity is elevated indoors (~ 12 ion pairs per $cm^3\,s^{-1}$), with concentrations that follow diurnal cycles affected by ventilation. The highest concentrations are observed at night, when there is little or no ventilation[30,41]. In this regard, caves are suitable locations to storing underground air with high radon activity[42], particularly, when the underground atmosphere has a low air renewal rate (for example, Castañar Cave[16,43]). It is expected that there will be a high density of ions in such environments, and this is borne out by the measurements made in the subterranean sites that were studied. The results derived from our continuous monitoring of radon activity in underground air confirm that CH_4 depletion occurs in underground air as it is enriched in radon (Fig. 6). The ratio of the concentrations of CO_2 and CH_4 is directly proportional to the intensity of ventilation process of the subsurface atmosphere, that is, the degree of cave air renewal through the inlet of air from exterior with the atmospheric levels of both the gases (CO_2 and CH_4). The ratio of the concentrations of CO_2 and CH_4 tends to zero once the radon concentration in underground air exceeds $2,000\,Bq\,m^{-3}$ (Fig. 6).

It is widely known that the photochemical oxidation of CH_4 in the troposphere is largely dominated by its reaction with hydroxyl radicals (OH). Under the majority of environmental conditions, the hydroxyl radical lifetime is less than a second[44]. Unlike the outdoor atmosphere, however, one of the important OH sources in indoor air may be from radioactive ^{222}Rn decay. An earlier study provided basic data for the evaluation of indoor radioactive pollution using chemical amplification techniques[45], quantifying the HOx production rate in indoor air from the radiolysis of water vapour by radon decay on an average rate of

$(4.31 \pm 0.07) \times 10^5$ HOx molecules per radon decay per second (Bq) over a range of relative humidity from 3.4 to 55.0% at 22 °C.

The ionic reactions of gaseous CH_4 with its each primary ion, including ions CH_4^+, CH_3^+, CH_2^+, CH^+ and C^+, represent other mechanism of CH_4 removal. An ion-molecule reaction mechanism is implicated in the formation of these upper homologues of CH_4, according to[46,47]:

$$CH_4^+ + CH_4 \rightarrow CH_5^+ + CH_3$$

$$CH_4^+ + CH_4 \rightarrow C_2H_4^+ + 2H_2$$

$$CH_4^+ + CH_4 \rightarrow C_2H_6^+ + H_2.$$
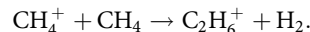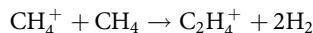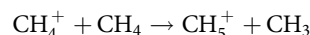
The starting point of this ion-molecule reaction mechanism is the CH_4^+ ion, which also appears under the action of uranium–radon (and its descendants) α-attack of CH_4 (ref. 48). In the case of ion-molecule reactions of O^+ with CH_4, other product ions are generated, such as OH^- and CH_4^+ (ref. 49). Therefore, the above-mentioned reactions for CH_4 removal by oxidation with hydroxyl radicals and ion-molecule reactions provide feedback to the system.

Overall, our findings contribute to a conceptual advance in our understanding of the CH_4 budget by including the subsurface-related CH_4 sink, which has long been largely overlooked. The discovery of frequent (daily), rapid (several hours) and complete CH_4 consumption in subsurface locations makes the uppermost portion of the vadose zone a special site for a CH_4 sink. CH_4 concentrations in underground air below the atmospheric background were found at all points inside the group of caves that was studied. In addition, rapid consumption of atmospheric CH_4 was observed in the underground air of dynamically ventilated caves (for example, Altamira Cave), just after the advective mixing of the cave air with exterior air. Therefore, sub-atmospheric CH_4 concentrations have not only been observed locally but are widespread the atmospheres of all the studied caves. The caves that were studied are distributed across a range of latitudes from 36–43° N to 0–5° W (Supplementary Fig. 1; Supplementary Table 1) and they have different geomorphological properties, different locations relative to the surface and different host-rock discontinuities. Our *in situ* measurements have also documented the link between CH_4 depletion and ion concentration in the subsurface atmosphere; however, the mechanism of CH_4 consumption remains a hypothesis to be tested by laboratory experimentation.

In light of these results, a new line of research could extrapolate to a global scale and analyse the CH_4 sink that has been described here for the subterranean atmosphere. There are early observations regarding CH_4 sinks in cave atmospheres that refer to other latitudes in the southern hemisphere, which are quite different to the locations in the north temperate zone that are described here. The phenomenon described here may thus be relevant on a global scale. CH_4 consumption of 1,000 p.p.b. in only a few hours was described in the subterranean air of an Australian cave, for example[26]. There are not yet enough globally representative data on CH_4 in subsurface atmospheres, so extrapolation of the CH_4-sink model to a global scale still entails much uncertainty. Part of what is estimated at present to be soil uptake may be due to subsurface atmosphere; therefore, the CH_4 sink suggested here is probably at present embedded in the soil uptake term of forward and inverse modelling studies. However, understanding the processes that control the generation, abundance and fate of CH_4 in the atmosphere, oceans and shallow crust is critical for understanding the future of the environment, because CH_4 is a naturally and anthropogenically emitted GHG[50]. Improved knowledge about the oxidation of CH_4 in the subsurface atmosphere under temperature and pressure

conditions characteristic of the troposphere near sea level ($+15\,°C$ and $103.15\,kPa$, respectively), could lead to the development, in the medium and long term, of technological alternatives for the removal or storage of GHGs, the identification of new cost-effective ways and methods for mitigation CH_4 emissions and the design of new strategies for atmospheric CH_4 elimination in underground environments. Therefore, different formation, transport and removal processes of CH_4 often impart distinctive isotopic fractionations and abundance of clumped isotopologues[51], which can provide information about the mechanisms involved and determine constraints on the sinks that can help guide future mitigation efforts. Finally, laboratory experiments should be conducted to attempt to reproduce the oxidation of CH_4 under different environmental conditions.

Methods

Environmental monitoring networks at fieldwork sites. Previous studies have demonstrated the availability of a wide set of facilities and devices that are especially designed to control, measure and analyse interesting parameters related to variations in cave environment conditions at each fieldwork site[16,17]. Further descriptions, technical data and results from the monitoring networks are found in these reports. These monitoring networks include sensors and data loggers continuously record local environmental parameters in cave air (pressure, temperature and relative humidity, wind speed and direction, air pressure and CO_2 and ^{222}Rn contents), soil (CO_2, temperature and moisture content) and the exterior atmosphere (rainfall, temperature, relative humidity, atmospheric pressure, solar radiation, wind speed and direction).

GHGs monitoring. A specific sampling and analysis programme for GHGs was implemented for each field site, including: (1) seasonal spot air-sampling and GHG analyses during short surveys at all fieldwork sites and (2) intensive field campaigns conducted for 38 h in the Castañar and Altamira caves, to obtain daily cycles of the GHG mixing ratio through comprehensive real-time logging using CRDS.

Spot air sampling was conducted seasonally in a predefined network of points spatially distributed inside each cave and during several short surveys (<3 h long). In total, 1,037 air samples were analysed for the seven caves studied, including 549 samples from cave air, 281 samples from soil air and 207 samples from atmosphere. Sampling was duplicated (morning/afternoon) in the most accessible and smaller caves. Exterior and soil air were sampled at fixed locations throughout the day, and, preferably, during maximum (midday) and minimum photosynthetic activity (early morning). Cave and atmosphere samples were taken 1 m above from the floor. Soil air collection was conducted at sites located vertically above each cave using a steel tube with grooved sides at its ends. The tubes were inserted to a depth of 20–50 cm near the bedrock–soil interface. Soil air was extracted using a micro-diaphragm gas pump (KNF Neuberger, Freiburg, Germany) at $3.1\,l\,min^{-1}$ at atmospheric pressure, and the pump was equipped with a 0.2-µm filter to avoid contamination with airborne particles. A portable air compressor (AQUANIC s790) was run at $0.4\,l\,min^{-1}$ for the cave air and atmosphere samples. Air samples were collected into 1L Tedlar bags with lock valves, especially designed to ensure the inertness and impermeability of air samples. Each air sample was purged at least one time with air from each sampling point to avoid contamination. Furthermore, the operator remained at a sufficient distance from the portable air compressor during the short interval needed for filling each 1L Tedlar bag, thereby avoiding any contamination by human breathing. The Picarro analyser works with a sample flow below $0.05\,s.l.m.$ (standard litre per minute, at 760 Torr) and it is only necessary 10 min for achieving a reliable measurement of the three parameters (CO_2, CH_4 and $\delta^{13}CO_2$), therefore <50 s of pumping is enough to provide a suitable volume of air (both from cave and exterior atmospheres) for subsequent analysis using the CRDS technique. Less than 20 s of pumping was enough to provide a suitable volume of soil air for subsequent analysis using the CRDS technique. Thus, we ensured that no air was taken in from the atmosphere. The bag samples were analysed within 48 h of sampling to determine CO_2 and CH_4 concentrations and the isotopic $\delta^{13}CO_2$ signal using a laser-based analyser that employs CRDS technology[52], as described below.

In situ and real-time measurements of CO_2, CH_4 and $\delta^{13}CO_2$ were carried out during an intensive field campaign of 38 h using a field-deployable CRDS analyser model G2101-i (Picarro Inc., Santa Clara, CA, USA). This fieldwork aimed to provide detailed records of GHG variations on short-term and diurnal timescales. Continuous monitoring of GHGs was conducted in the Altamira cave, for which a previous complete environmental database regarding cave processes exists. The field campaign was deployed during the warm, dry period at the end of the summer, when the cave is most tightly coupled with the external atmosphere and ventilation is at its most effective[24,25]. A detailed time series of GHGs content was obtained (>1,18,000 records with data of $^{12}CO_2$ and $^{13}CO_2$ contents every 2 s), covering a monitoring period of 38 h (two night-time periods and one daytime period, from day 19 until 21 September 2011). The $\delta^{13}C–CO_2$ value was automatically calculated using the CRDS analyser by the raw measurements of

$^{12}CO_2$ and $^{13}CO_2$ concentration and by taking a central moving average with a window of 5 min, which provides suitable precision according to the manufacturer's specifications. In addition, a comprehensive network of monitoring stations was specifically implemented to register the coeval short-term environmental changes, including parameters such as air temperature, relative humidity, air pressure and radon contents. The CRDS analyser was operated in continuous mode with a network of tubes connected to a multivalve sequencer, which enabled simultaneous air sampling from different locations (cave, soil and atmosphere) for >10 min each time by alternating the opening and closing of valves. Air from each location was pumped using a 4-mm (inner diameter) polyurethane tube from the main galleries of each cave site and using a micro-diaphragm gas pump as described above. An air extraction tube was connected to the analyser using a T-connection to avoid problems related to overpressure effects. As an alternative to continuous gas monitoring, sampling bags of exterior and soil air were also collected throughout the day.

Analyses of GHGs using both the procedures (spot-sampling bags and continuous real-time monitoring) were performed using a CRDS analyser Picarro G2101-i (Picarro Inc.). This analyser performs *in situ* and real-time measurements of atmospheric levels of carbon dioxide ($^{12}CO_2$ and $^{13}CO_2$), CH_4 and water vapour (H_2O_v). The isotopic $\delta^{13}CO_2$ relationship is automatically measured as a calculation based on $^{12}CO_2$ and $^{13}CO_2$ concentrations and considering a correction due the presence of other target species (CH_4 and H_2O_v). Precisions of 200 and 10 p.p.b. are guaranteed by the manufacturer for $^{12}CO_2$ and $^{13}CO_2$, respectively, over a wide operating range, with a resulting precision of <0.3‰ for $\delta^{13}C(CO_2)$ after 5 min of analysis. The maximum drift of $\delta^{13}C(CO_2)$ is <2.0‰ over 24 h at standard air pressure (peak to peak, 1 h average). Periodic tests were conducted to check that the analyser achieved the above performance specifications (precision and drift) in accordance with the guidelines of the manufacturer (test for 24 uninterrupted hours using the analyser attached to a cylinder of compressed air with known GHG abundances). Measurements of CO_2 in air were performed relative to three reference standards whose gas mixing ratio was determined with high precision and accuracy. On each day/session of analysis using the CRDS analyser (field deployment or analysis of air bags in the lab), the internal secondary standards were run regularly, at least at the beginning and at the end of the analyses, to verify the proper functioning of the analyser. This procedure periodically confirmed that the performance specifications regarding CO_2 analyses via CRDS were met. Regarding CH_4 measurements, the instrument's response to the sample was also compared with three standards with known CH_4 contents. The measurement accuracy determined through repeated analysis of CH_4 in standard gas cylinders was <0.1 p.p.m. in the studied range of levels (0–2 p.p.m.). In addition, CH_4 measurements was corrected as a function of the presence of H_2O_v through periodical calibrations of the analyser using synthetic gases with known CH_4 abundances (0, 0.5 and 1.7 p.p.m.v.) over a wide range of H_2O_v levels (0–3.5%).

In addition, some initial spot measurements of air ion density were conducted in Castañar cave to test the range of values in underground air with null CH_4 concentration. A handled air ion counter was used (AlphaLab Air Ion Counter). This instrument is a true ion density metre, based on a Gerdien Tube (Gerdien Condenser) design, and it contains a fan that pulls air through the metre at a calibrated rate. The Air Ion Counter is designed to measure density of ions, that is, the number of ions per cubic centimetre in air, accomplishing the following performance specifications: range: $0–2 \times 10^7$ ions per m^3; resolution: 10 ions per m^3; accuracy: ± 25% of the reading; and response time: 2 s. It also measures this number separately for positive and negative ions.

In light of these preliminary observations, a detailed multiparametric and spatially resolved monitoring of air ions density was conducted during a specific field survey in Ojo Guareña cave, in tandem with the analysis of gas composition (CH_4, CO_2 and $\delta^{13}C–CO_2$) and microclimatic parameters (temperature and relative humidity) in the underground air, the soil air and the external atmosphere.

For this study, continuous monitoring (every half hour) of changes in the radon concentration in the underground air was conducted at three cave sites: Castañar, Altamira and Ojo Guareña. Several Radim 5WP monitors (SMM Company, Prague, Czech Republic and distributed by GT-Analytic KG Innsbruck, Austria) were used, because these monitors are mainly designed for indoor radon measurements. These monitors determine radon concentration by measuring gross α-activity of the radon decay products ^{218}Po and ^{214}Po, which are collected electrostatically on the surface of a Si-semiconductor. The lowest activity detectable is $80\,Bq\,m^{-3}$ for 1-h measurements with a statistical error equal to ± 20%. The maximum detectable activity is $150\,kBq\,m^{-3}$. The instrument response is $0.4\,(imp\,h^{-1})/(Bq\,m^{-3})$. The monitors were periodically calibrated by the manufacturer. In addition, the monitors were checked regularly in the field (inside the caves) using a Pylon AB5 scintillator photomultiplier with a continuous passive radon detector (Pylon Electronics Inc., Ottawa, Canada) as a reference instrument. This reference instrument was periodically calibrated to provide highly accurate measurements (lowest detectable activity: $24.8\,Bq\,m^{-3}$, with a sensitivity of $0.041\,c.p.m.\,(Bq\,m^{-3})^{-1}$, accuracy of ± 4% and nominal background of $0.4\,c.p.m.$).

MOBs tracking. Microbiological sampling was conducted to assess the presence or absence of MOBs in the edaphic profile at exterior and sediments and rock surfaces into cave from each monitored field site. Inside caves, samples were collected in the

cave entrance and in the most remote but accessible locations. Sampling was carried out using sterilized materials. On collection, the samples were stored on ice and processed on arrival to the laboratory. Collected samples were analysed by an ordered set of techniques: nucleic acid extraction and PCR amplification, cloning and sequencing and sequence analyses[53].

Nucleic acid extraction and PCR amplification. Extraction of total nucleic acids from the samples was performed using the method proposed by Griffiths *et al.*[54] in conjunction with a FastPrep instrument, according to the manufacturer's instructions. Extracted nucleic acids were resuspended in 50 ml of sterile ultrapure water (Sigma-Aldrich). For RNA extraction, a 25-ml aliquot was subjected to a DNase digestion step using a RNase-Free DNase (Qiagen), and the purification of RNA using the RNeasy MinElute Cleanup kit (Qiagen), according to the manufacturer's instructions. Superscript II Reverse Transcriptase (Invitrogen) was used to synthesize complementary DNA (cDNA) using specific primers: Mb661 (5′-CCG GMG CAA CGT CYT TAC C-3′) and A682 (5′-GAA SGC NGA GAA GAA SGC-3′) for bacterial *pmoA* gene[55,56] and 1492R (5′-GGY TAC CTT GTK WCG ACT T-3′) for bacterial 16S rRNA gene[57] at a temperature of 42 °C for 50 min. Amplification of cDNA will be performed with the methanotrophs-specific primer pairs: A189F (5′-GGN GAC TGG GAC TTC TGG-3′)/Mb661, and A189F/A682 (ref 55), and a universal bacterial primer: 27F (5′-AGA GTT TGA TCC TGG CTC AG-3′)/1492R (ref 56). One or 2 ml of cDNA, diluted 1/10 was used as a template. PCR conditions were the same for DNA. PCR reactions were performed in a Bio-Rad iCycler thermal cycler (Bio-Rad). The PCR reaction mixture (1 ml) contains 100 ml of PCR buffer (Biotools), 30 ml of MgCl2 (50 mM, Biotools), 10 ml of each primer (50 mM), 100 ml of dNTPs (100 mM, Bioline), 5 ml of Taq polymerase (Biotools) and 750 ml of sterile ultrapure water. The thermal cycler for PCR amplification consisted of 94 °C for 4 min; 28 cycles of 94 °C for 1 min, 56 °C for 1 min (45 °C for 27F/1492R), 72 °C for 45 s; and a final step of 72 °C for 5 min. Positive and negative controls were included in all amplification experiments. All amplification products were purified using a JETquick PCR Purification Spin kit (Genomed) and stored at −20 °C for further analysis.

Cloning and sequencing. DNA libraries of PCR amplified products were constructed using the pGEM-T Easy Vector (Promega) and then transformed into One Shot Max Efficiency DH5a-T1 chemically competent *Escherichia coli* (Invitrogen) according to the manufacturer's instructions. Transformants were randomly picked and transferred to other plates containing Luria–Bertani medium supplemented with 100 mg ml^{-1} ampicillin and 15% w/v glycerol and stored at −80 °C. The amplicons that contain the correct size of *pmoA* and 16S rRNA genes fragment were re-amplified using the primer pairs as described above. On average, 100 clones from each library were sequenced at Macrogen Inc., Korea.

Sequence analyses. Low-quality (short) sequences were removed from the data set. Sequences were aligned using the software package _other[58]. Sequences were checked for chimera by chimera.slayer as implemented in _other. Putative chimeric sequences were excluded from further analysis. After this analysis, all sequences were compared with the non-redundant database of sequences deposited at the National Center for Biotechnology and EzTaxon[59] using BLASTN algorithm[60]. Aligned sequences were clustered into operational taxonomic units using _other, with a 97% sequence identity cutoff for 16S rDNA sequence and 93% for *pmoA* sequence[61]. Rarefaction curves and Venn diagrams were also obtained using _other.

References

1. Dlugokencky, E. J. *et al.* Observational constraints on recent increases in the atmospheric CH$_4$ burden. *Geophys. Res. Lett.* **36,** L18803 (2009).
2. Bousquet, P. *et al.* Contribution of anthropogenic and natural sources to atmospheric methane variability. *Nature* **443,** 439–443 (2006).
3. Chen, Y. H. & Prinn, R. G. Estimation of atmospheric methane emissions between 1996 and 2001 using a three-dimensional global chemical transport model. *J. Geophys. Res.* **111,** D10307 (2006).
4. Khalil, M. A. K., Butenhoff, C. L. & Rasmussen, R. A. Atmospheric methane: trends and cycles of sources and sinks. *Environ. Sci. Technol.* **41,** 2131–2137 (2007).
5. Heimann, M. Atmospheric science: enigma of the recent methane budget. *Nature* **476,** 157–158 (2011).
6. Dlugokencky, E. J., Nisbet, E. G., Fisher, R. & Lowry, D. Global atmospheric methane: budget, changes and dangers. *Philos. Trans. A Math. Phys. Eng. Sci.* **369,** 2058–2072 (2011).
7. Hartmann, D. L., Klein, A. M. G. & Rusticucci, M. in *Climate Change 2013: The Physical Science Basis.*. (eds Stocker, T. F. *et al.*) 159–254 (Cambridge Univ. Press, 2013).
8. Ciais, P. & Sabine, C. in *Climate Change 2013: The Physical Science Basis* (eds Stocker, T. F. *et al.*) 465–570 (Cambridge Univ. Press, 2013).
9. Lelieveld, J., Crutzen, P. J. & Dentener, F. J. Changing concentration, lifetime and climate forcing of atmospheric methane. *Tellus* **50B,** 128–150 (1998).
10. Myhre, G. & Shindell, D. in *Climate Change 2013: The Physical Science Basis.*. (eds Stocker, T. F. *et al.*) 659–740 (Cambridge Univ. Press, 2013).
11. Fisher, R. E. *et al.* Arctic methane sources: Isotopic evidence for atmospheric inputs. *Geophys. Res. Lett.* **38,** L21803 (2011).
12. Montzka, S. A., Dlugokencky, E. J. & Butler, J. H. Non-CO$_2$ greenhouse gases and climate change. *Nature* **476,** 43–50 (2011).
13. Smith, R. N. B. *Subsurface, surface and boundary layer processes.* 1–54. Unified Model Documentation Paper 24 (NCAS-CMS Climate Research Meteorological Office) (1996).
14. Atkinson, T. C. CO$_2$ in the atmosphere of the unsaturated zone: an important control of groundwater hardness in limestones. *J. Hydrol.* **35,** 111–123 (1977).
15. Serrano-Ortiz, P. *et al.* Hidden, abiotic CO$_2$ flows and gaseous reservoirs in the terrestrial carbon cycle: review and perspectives. *Agric. For. Meteorol* **150,** 321–329 (2010).
16. Fernandez-Cortes, A. *et al.* Characterization of trace gases' fluctuations on a 'low energy' cave (Castañar de Ibor, Spain) using techniques of entropy of curves. *Int. J. Climatol.* **31,** 127–143 (2011).
17. Cuezva, S. *et al.* Short-term CO$_2$(g) exchange between a shallow karstic cavity and the external atmosphere during summer: role of the surface soil layer. *Atmos. Environ.* **45,** 1418–1427 (2011).
18. Garcia-Anton, E., Cuezva, S., Fernandez-Cortes, A., Benavente, D. & Sanchez-Moral, S. Main drivers of diffusive and advective processes of CO$_2$-gas exchange between a shallow vadose zone and the atmosphere. *Int. J. Greenh. Gas Control* **21,** 113–129 (2013).
19. Bourges, F., Genthon, P., Genty, D., Mangin, A. & D'Hulst, D. Comment on "Carbon uptake by karsts in the Houzhai Basin, southwest China" by Junhua Yan *et al. J. Geophys. Res.* **117,** 1–3 (2012).
20. Holmes, A. J. *et al.* Characterization of methanotrophic bacterial populations soils showing atmospheric methane uptake. *Appl. Environ. Microbiol.* **65,** 3312–3318 (1999).
21. Ek, C. & Gewelt, M. Carbon-dioxide in cave atmospheres. New results in Belgium and comparison with some other countries. *Earth Surf. Proc. Land.* **10,** 173–187 (1985).
22. Bourges, F., Mangin, A. & D'Hulst, D. Le gaz carbonique dans la dynamique de l'atmosphère des cavités karstique: l'exemple de l'Aven d'Orgnac (Ardèche). *Earth Planet. Sci. Lett.* **333,** 685–692 (2001).
23. Fernandez-Cortes, A. *et al.* in *Hydrogeological and Environmental Investigations in Karst Systems, Environmental Earth Sciences.* (eds Andreo, B. *et al.*) 523–531 (Springer-Verlag, 2015).
24. Sanchez-Moral, S. *et al.* Inorganic deterioration affecting the Altamira Cave, N Spain: quantitative approach to wall-corrosion (solutional etching) processes induced by visitors. *Sci. Total Environ.* **243/244,** 67–84 (1999).
25. Kowalski, A. S. *et al.* Can flux tower research neglect geochemical CO2 exchange? *Agric. For. Meteorol.* **148,** 1045–1054 (2008).
26. Waring, C. L., Griffith, D. W. T., Wilson, S. & Hurry, S. Cave atmosphere: A guide to calcification and a methane sink. *Geochim. Cosmochim. Acta* **73,** A1419–A1419 (2009).
27. Mattey, D. P. *et al.* Methane in underground air in Gibraltar karst. *Earth Planet. Sci. Lett.* **374,** 71–80 (2013).
28. Hirsikko, A. *et al.* Atmospheric ions and nucleation: a review of observations. *Atmos. Chem. Phys.* **11,** 767–798 (2011).
29. Sas, D., Sladek, P. & Navratil, O. Radon and air ion balance. *Czech. J. Phys.* **56,** D141–D148 (2006).
30. Hirsikko, A. *et al.* Indoor and outdoor air ions and aerosol particles in the urban atmosphere of Helsinki: characteristics, sources and formation. *Boreal Environ. Res.* **12,** 295–310 (2007).
31. Junninen, H. *et al.* Observations on nocturnal growth of atmospheric clusters. *Tellus* **60B,** 365–371 (2008).
32. Winkler, P. M. *et al.* Heterogenous nucleation experiments bridging the scale form molecular ion cluster to nanoparticles. *Science* **7,** 1374–1377 (2008).
33. Laakso, L., Mäkelä, J. M., Pirjola, L. & Kulmala, M. Model studies on ion-induced nucleation in the atmosphere. *J. Geophys. Res.* **107,** 4427 (2002).
34. Yu, F. Ion-mediated nucleation in the atmosphere: Key controlling parameters, implications, and look-up table. *J. Geophys. Res.* **115,** D03206 (2010).
35. Luts, A. & Parts, T. Evolution of negative small air ions at two different temperatures. *J. Atmos. Sol. Terr. Phys.* **64,** 763–774 (2002).
36. Dhanorkar, S. & Kamra, A. K. Diurnal variation of ionization rate close to ground. *J. Geophys. Res.* **99,** 18523–18526 (1994).
37. Nagaraja, K., Prasad, B. S. N., Madhava, M. S. & Paramesh, L. Concentration of radon and its progeny near the surface of the earth at a continental station Pune (18_ N, 74_ E). *Ind. J. Pure Appl. Phys.* **41,** 562–569 (2003).
38. Horrak, U., Salm, J. & Tammet, H. Diurnal variation in the concentration of air ions of different mobility classes in a rural area. *J. Geophys. Res.* **108,** 4653 (2003).
39. Tammet, H., Hõrrak, U., Laakso, L. & Kulmala, M. Factors of air ion balance in a coniferous forest according to measurements in Hyytiälä, Finland. *Atmos. Chem. Phys.* **6,** 3377–3390 (2006).
40. Kolarz, P. M., Filipovic, D. M. & Marinkovic, B. P. Daily variations of indoor air-ion and radon concentrations. *Appl. Radiat. Isot.* **67,** 2062–2067 (2009).

41. Fews, A. P., Holden, N. K., Keitch, P. A. & Henshaw, D. L. A novel high-resolution small ion spectrometer to study ion nucleation of aerosols in ambient indoor and outdoor air. *Atmos. Res.* **76,** 29–48 (2005).

42. Cigna, A. A. Radon in caves. *Int. J. Speleol.* **34,** 1–18 (2005).

43. Lario, J., Sanchez-Moral, S., Cuezva, S., Taborda, M. & Soler, V. High ^{222}Rn levels in a show cave (Castañar de Ibor, Spain): proposal and application of management measures to minimize the effects on guides and visitors. *Atmos. Environ.* **40,** 7395–7400 (2006).

44. Monks, P. S. Gas-phase radical chemistry in the troposphere. *Chem. Soc. Rev.* **34,** 376–395 (2005).

45. Ding, H. & Hopke, P. K. HOx production due to radon decay in air. *J. Atmos. Chem.* **17,** 375–390 (1993).

46. Haynes, R. M. & Kebarle, P. Mass-spectrometric study of ions at near-atmospheric pressure. The alpha radiolysis of methane. *J. Chem. Phys.* **45,** 3899–3906 (1966).

47. Rasul, G., Surya Prakash, G. K. & Olah, G. A. Comparison of structures and energies of CH52 + with CH4 + and their possible role in supercidic methane activation. *Proc. Nat Acad. Sci. USA* **94,** 11159–11162 (1997).

48. Cosma, C., Suciu, I., Jantschi, L. & Bolboaca, S. Ion-molecule reactions and chemical composition of emanated from herculane spa geothermal sources. *Int. J. Mol. Sci.* **9,** 1024–1033 (2008).

49. Ottinger, C. H., Zimmerann, S. & Muschlitz, E. E. Ion-molecule reactions of O + with CH$_4$. *Chem. Phys.* **81,** 211–220 (1983).

50. Wuebbles, D. J. & Hayhoe, K. Atmospheric methane and global change. *Earth Sci. Rev.* **57,** 177–210 (2002).

51. Stolper, D. A. *et al.* Combined 13C–D and D–D clumping in methane: methods and preliminary results. *Geochim. Cosmochim. Acta* **126,** 169–191 (2014).

52. Crosson, E. R. A cavity ring-down analyzer for measuring atmospheric levels of methane, carbon dioxide, and water vapor. *Appl. Phys. B* **92,** 403–408 (2008).

53. Diaz-Herraiz, M. *et al.* Deterioration of an Etruscan tomb by bacteria from the order *Rhizobiales*. *Sci. Rep.* **4,** 3610 (2014).

54. Griffiths, R. I., Whiteley, A. S., O'Donnell, A. G. & Bailey, M. J. Rapid method for coextraction of DNA and RNA from natural environments for analysis of ribosomal DNA- and rRNA-based microbial community composition. *Appl. Environ. Microbiol.* **66,** 5488–5491 (2000).

55. Costello, A. M. & Lidstrøm, M. E. Molecular characterization of functional and phylogenetic genes from natural populations of methanotrophs in lake sediments. *Appl. Environ. Microbiol.* **65,** 5066–5074 (1999).

56. Holmes, A. J., Costello, A. M., Lidstrom, M. E. & Murrell, J. C. Evidence that particulate methane monooxygenase and ammonia monooxygenase may be evolutionarily related. *FEMS Microbiol. Lett.* **132,** 203–208 (1995).

57. Pasic, L., Kovce, B., Sket, B. & Herzog-Velikonja, B. Diversity of microbial communities colonizing the walls of a Karstic cave in Slovenia. *FEMS Microbiol. Ecol.* **71,** 50–60 (2010).

58. Schloss, P. D. *et al.* Introducing mothur: Open-source, platform-independent, community-supported software for describing and comparing microbial communities. *Appl. Environ. Microbiol.* **75,** 7537–7541 (2009).

59. Kim, O. S. *et al.* Introducing EzTaxon-e: a prokaryotic 16S rRNA gene sequence database with phylotypes that represent uncultured species. *Int. J. Syst. Evol. Microbiol.* **62,** 716–721 (2012).

60. Altschul, S. F., Gish, W., Miller, W., Myers, E. W. & Lipman, D. J. Basic local alignment search tool. *J. Mol. Biol.* **215,** 403–410 (1990).

61. Degelmann, D. M., Borken, W., Drake, H. L. & Kolb, S. Different atmospheric methane-oxidizing communities in European beech and Norway spruce soils. *Appl. Environ. Microbiol.* **76,** 3228–3235 (2010).

62. Dlugokencky, E. J., Lang, P. M., Crotwell, A. M., Masarie, K. A. & Crotwell, M. J. *Atmospheric Methane Dry Air Mole Fractions from the NOAA ESRL Carbon Cycle Cooperative Global Air Sampling Network, 1983–2012* ftp://aftp.cmdl.noaa.gov/data/trace_gases/ch4/flask/surface/ (2013).

63. Dlugokencky, E. J., Lang, P. M., Masarie, K. A., Crotwell, A. M. & Crotwell, M. J. *Atmospheric Carbon Dioxide Dry Air Mole Fractions from the NOAA ESRL Carbon Cycle Cooperative Global Air Sampling Network, 1968–2012* ftp://aftp.cmdl.noaa.gov/data/trace_gases/co2/flask/surface/ (2013).

Acknowledgements

Author contributions

All authors contributed extensively to the work presented in this paper. A.F-C and S.C. have contributed equally to the work, oversaw all fieldwork, designed the research and edited the manuscript. M.A-G., E.G-A, C.P. and D.B. participated in the collection and analysis of samples and data. V.J. and C.S-J. performed the microbiological analyses and the interpretation of microbiological data. S.S-M. conceived and supervised the study. All authors have discussed the results and implications and commented on the manuscript at all stages.

Additional information

Supplementary Information accompanies this paper at http://www.nature.com/naturecommunications

Competing financial interests: The authors declare no competing financial interests.

Reprints and permission information is available online at http://npg.nature.com/reprintsandpermissions/

How to cite this article: Fernandez-Cortes, A. *et al.* Subterranean atmospheres may act as daily methane sinks. *Nat. Commun.* 6:7003 doi: 10.1038/ncomms8003 (2015).